Kurdish Studies
March 2023
Volume: 11, No: 1, pp. 521-539
ISSN: 2051-4883 (Print) | ISSN 2051-4891 (Online)
www.KurdishStudies.net

Received: January 2023 Accepted: February 2023
DOI: 10.53555/ks.v11i1.2945

Effect of High Temperature on the Microstructure ad Mechanical Properties of Eco-Friendly Hybrid Fibre Reinforced Geopolymer Concrete (HFRGPC): An Experimental and Modelling Study

Jooyandeh Mirza A[1]*, Alizadeh Elizei M.H[2], Adabi M[3]

[1]PhD student in Civil Engineering, Faculty of ,Roudehen Branch, Islamic Azad University, Roudehen, Tehran,Iran.

[2]Assistant Professor of Civil Engineering - StructurEngineeringe (Corresponding Author), Faculty of Engineering,Roudehen Branch, Islamic Azad University, Roudehen, Tehran,Iran.

[3]Assistant Professor, Department of Metallurgy and Materials Engineering, Faculty of Engineering, Roudehen Branch, Islamic Azad University, Roudehen, Tehran,Iran.

***Corresponding Author:** Jooyandeh Mirza A
*PhD student in Civil Engineering, Faculty of Engineering, Islamic Azad University of Roodehen, Damavand, Iran.

ABSTRACT:
This study aims to investigate the effects of metakaolin (MK) and natural zeolite (NZ) on the properties of a fibre reinforced fly ash-based geopolymer concrete containing 100% recycled coarse aggregate from crushed specimens of laboratory. Polypropylene fibre (PF) with volume fractions of 0, 0.5, 1, and 1.5% and steel fibre with constant volume fraction as reinforcement in geopolymer concrete (HFRGPC) were added into the mixes to improve the overall mechanical properties. In this study, workability, compressive strength, splitting tensile strength and modulus of elasticity tests were conducted to investigate the behaviours of HFRGPC at room temperature. Moreover, the fire resistance of the HFRGPC mixes with optimum value of PF is studied in term of residual compressive strength. The results indicate that the combined effect of the 20% MK substitution and 1% PF inclusion in the HFRGPC mixes exhibited the largest compressive strength (52.7 MPa), modules of elasticity (30.6 GPa), and splitting tensile strength (5.7 MPa). In addition, the HFRGPC containing 20% MK and 1% PF maintained the residual compressive strength of 32.64 MPa at 700 °C, and thus recording a minimum strength loss of 38%. Subsequently, a robust machine learning model is developed to formulate the compressive strengths of HFRGPC under high temperature. Results indicated that the machine learning-based prediction model provide powerful tools to simulate the compressive strength of HFRGPC subjected to different temperatures. The results of ANOVA also show that temperature has a major influence on the compressive strength of HFRGPC, with percent contributions of 71.98% and the lowest contribution related to NZ with 5.52%.

PRACTICAL APPLICATIONS:
In this research, by adding pozzolanic materials such as metakaolin and zeolite instead of fly ash, they each have their own effect on compressive strength, tensile strength and modulus of elasticity, causing them to increase or decrease, so that some have an unfavorable effect and some have a favorable effect. had Adding the optimal amount of polypropylene fibers to improve the resistance properties of this concrete has given a favorable response and improved them. But as for the temperature, as the temperature increases, 200 and 400 degrees Celsius, the compressive strength increases, but as the temperature increases up to 700 degrees Celsius, the compressive strength decreases. In the machine modeling method, ML techniques showed that it is accurate and valid through experimental compressive strength values in the training and testing phase and in terms of correlation coefficient, while the formula proposed by the decision tree model showed less errors in the testing phase.

AUTHOR KEYWORDS: Hybrid Fibre-Reinforced Geopolymer Concrete, Polypropylene Fibre, High Temperature, Machine Learning, Prediction Model

INTRODUCTION:

The global construction growth has led to an increase in the demand for concrete, which still depends mainly on ordinary Portland cement (OPC). Roughly 3.6 billion tons of cement are produced each year in the world and each ton of concrete emits approximately 0.9 ton of CO_2 (Environment et al. 2018; Bhogayata et al. 2020). Moreover, about 1.5 tons of raw materials are used to produce one ton of OPC (Amran et al. 2020); therefore, the necessity for an alternative to OPC-based materials was sensed to address these problems. geopolymers are known as environmentally friendly alternatives to OPC-based materials (Erfanimanesh and Sharbatdar 2020; Top et al. 2020). Due to reduced energy consumption and less CO_2 emission during the manufacture, geopolymers received considerable attention over Portland cement in recent years (Singh and Middendorf 2020; Chen et al. 2021; Shehata et al. 2021). The geopolymers are attractive as green concrete in construction industry because of cost efficiency, chemical stability, corrosion resistance, rapid strength gain rate, low density, low permeability, low shrinkage and freeze-thaw resistance (Pradhan et al. 2022; Jindal et al. 2023). The geopolymers are amorphous cementitious binders having cross-link chain of silica, oxygen and alumina (Si-O-Al) (Suwan et al. 2016; Mahmoodi et al. 2021). They are synthesized by reacting aluminosilicate source materials (i.e. metakaolin, fly ash, blast furnace slag, etc) with highly alkaline activators. Further, the chemical composition, mineralogical composition, morphology, fineness and glassy phase content present in aluminosilicate sources decide the microstructures and mechanical properties of geopolymers (Turner and Collins 2013).

The metakaolin based geopolymer offers better strength, permeability, etc. However, it has limitations of poor rheological properties due to plate shaped morphology, complex processing, higher water demand, accelerated hydration reactions and more heat evolved at early ages (Albidah et al. 2021; Jindal et al. 2023). On the contrary, fly ash-based geopolymer is more durable and stronger than that of metakaolin-based geopolymer. However, it also has disadvantages such as extended setting times, slow strength development, low early-age strength, construction delay, difficulties to use in cold weather concreting, etc. (Singh and Middendorf 2020). It can be concluded from the abovementioned concerns, combination of the pozzolanic materials such as metakaolin and fly ash may solve many drawbacks of geopolymer concrete such as durability, bond behaviour, and high temperature resistance. Despite many benefits, geopolymers still have certain limitations over ordinary Portland cement. Due to their cross-linked structure, geopolymers tend to be more brittle, susceptible to crack formation and undergo catastrophic failure as compared to ordinary Portland cement (Deb et al. 2014; Shaikh and Hosan 2016).

Fibre reinforced concrete has been developed over the last few decades. The primary reason of addition of fibres in concrete is to improve its tensile and flexural strengths and post-cracking ductility. Different types of fibre including polypropylene fibre (PF) (Ranjbar et al. 2016; Tayeh et al. 2022), steel fibre (Dias and Thaumaturgo 2005; Lee et al. 2017), carbon fibre (Vilaplana et al. 2016; Wang et al. 2023), polyvinyl alcohol (PVA) fibre (Tanyildizi and Yonar 2016; Zanotti et al. 2017), basalt fibre (Dias and Thaumaturgo 2005) and polyethylene fibre (Choi et al. 2016; Lee et al. 2017) have been used for this purpose. Patil and Patil (2015) studied the PF-reinforced GPC with the ratio of alkaline liquids to fly ash of 5, sodium hydroxide solution to sodium silicate solution of 2.5. It was found that the compressive strength, split tensile strength and flexural strength of GPC increased by 8.483%, 12.259% and 19.250% respectively by adding 1.5 vol% 20 mm PF when compared to plain GPC. Aslani and Kelin (2018) found that the addition of the low percentage of PF could increase the mechanical performance of the fly ash-based matrix but reduced at a higher percentage of PF. Ranjbar et al. [18]gave that the inclusion of PF negatively impacted flexural strength, but positively influenced the energy absorption in comparison to plain GPC. Rickard et al. (2013) reported that the use of PF can reduce the density of GPC but decreased the compressive strength from 54 MPa to 36 MPa. Beside its advantages, PF is a low tensile strength and hydrophobic material, which lead to weak contact with the geopolymer binder, and could weaken the mechanical properties of the GPC at high fibre content (Aydin and Baradan 2013; Aslani and Kelin 2018; Rajak and Rai 2019).

In contrast, steel fibre behaves as a hydrophilic material and has strong contact with the geopolymer binder, which significantly improves the energy absorption and flexural strength of geopolymer composites (Ranjbar et al. 2016; Wang et al. 2020). Gülsan et al. (2019) reported that the addition of steel fibre into GPC significantly enhanced bond strength and flexural performance of GPC. Anna and Sumathi (2018) compared the durability characteristic of steel fibre-reinforced GPC, GPC and normal concrete, and found that the durable performance of steel fibre-reinforced GPC surpassed that of GPC, which was in turn better than that of normal concrete. Ranjbar et al. (2016) studied the effect of micro steel fibre on mechanical characteristics of fly ash-based geopolymer composites and stated that the incorporation of steel fibre into GPC improved ultimate flexural strength and energy absorption capacity. In addition, in many studies polymeric fibres reinforced concrete shows spalling resistance at fire, however, its post fire residual mechanical properties are of great concern, as these fibres are melting at elevated temperatures or lose their properties significantly if not melted. An advantage of steel fibre as one of the appropriate reinforcing materials in concrete at elevated temperature during fire is their inherent higher melting temperature than the polymeric fibres, due to which the steel fibre-reinforced concrete shows higher retention capacity of its original mechanical properties than its counterpart polymeric fibres reinforced concrete (Aslani and Kelin 2018). Mastali et al. (2019) investigated the fire resistance of alkali activated slag mortar reinforced with different types of fibers up to a temperature of 600 ^{o}C. They reported that the minimum compressive and flexural strengths reduction was recorded for the steel fiber-reinforced mix and basalt fiber-reinforced mix showed the lowest strength loss among the non-metallic fibers. Whereas, the highest strength loss was observed in PVA-reinforced counterparts. Abdollahnejad et al. (2021) studied the effects of reinforcing one-part alkali-activated slag binders with different types of fibres including PVA, steel, basalt, and cellulose fibres on the mechanical properties and durability such as

high temperature resistance. The incorporation of fibres had a substantial influence on the high-temperature resistance. The maximum residual strength belonged to the specimens reinforced with steel fibres.
The favourable influences of fibre reinforcement on cementitious materials exposed to elevated temperature mainly depend on the properties of fibres, the bond between fibre–matrix at interfacial transition zone (ITZ), and the matrix itself. According to the available literature, studies on the combined effects of both cementitious materials and fibre reinforcement of GPC, HFRGPC, under elevated temperature at different volume fractions are scarce. In this regard, keeping steel fibre constant, the optimum amount of PF along with metakaolin (MK) and natural zeolite (NZ) variations in the HFRGPC at 7 and 28-days of age is determined through slump, compressive strength, modules of elasticity, and splitting tensile strength tests. Moreover, different behaviour of steel and polypropylene fibres in the room temperature and after exposure to 200, 500, and 800 ˚C is investigated by residual compressive strength and the effect of fire exposure on the appearance and microstructure of HFRGPC mixes was evaluated by visual inspection and performing scanning electron microscopy (SEM). Finally, the experimentally developed database is utilized to train and establish two machine learning (ML) prediction model for the compressive strength of HFRGPC. The advantage of the muddling and extracting new formulation is that it eliminates the necessity of performing costly and time-consuming experiments. Additionally, it provides a useful tool to investigate the effect of parameters on the residual strength of HFRGPC, which might not be easily plausible via laboratory testing. The results of this study give a proper knowledge for choosing the content of cementitious materials and PF for the materials which are exposed to elevated temperature.

MATERIALS AND METHODS

Materials

In this study, the low calcium FAsh with a granule density of 2665 kg/m^3 was maintained from Foolad Mobarakeh Co. in Esfahan. In addition, the used Clinoptilolite type of zeolite (NZ) was supplied from Semnan mines in Iran, and had a specific gravity of 2140 kg/m^3 and Blaine fineness of 6788 cm^2/g. Moreover, Delijan MK was used as pozzolan which was supplied from the Ferro Alloy Industries Co. having a granule density of 2590 kg/m^3. The chemical properties and loss on ignition (LOI) of the used pozzolans are given in Table 1. Moreover, Figure 1 presented the X-ray diffraction (XRD) test for used SCMs.
The alkaline solution used in the presented study to activate the SCM (e, g., FAsh, MK and Z) was a compound of glass water (sodium silicate or Na_2SiO_3) and sodium hydroxide (NaOH). The solid sodium hydroxide 96% was prepared as a water-soluble solution. The sodium silicate solution utilized in this research had a SiO_2 / Na_2O ratio equal to 2.27 (SiO_2 = 35.9%, Na_2O = 15.8 %,). The experimental investigation for development of eco-friendly and structural GPC mixtures were performed using 2-part hybrid fibers namely steel (SF) and (PF). Table 2 referred the details of used fibers. The PF length of 6 mm was utilized to reinforce the GPC. Moreover, in this study, the hooked-end SF having a maximum length equal to 5mm and a diameter equal to 0.12 mm were used to develop and propose the optimal blends. To do so, PF at 0.5, 1, 1.5 vol% and SF at 2 vol%, were added in GPC mixture proportions.
The natural sand used as fine aggregate (FA) was prepared from a local quarry having a fineness modulus equal to 3.05, which was in the recommended range by ASTM C33. Recycled aggregate from crushed structural concrete obtained from the strength test in laboratory with compressive strengths of 30–40 MPa is used as the coarse aggregate (CA) in this study. The concrete samples were crushed and sieved into 2.8–12.5 mm particle size. Also, the specific gravity and water absorption values were equal to 2.57 and 1.52%, respectively. Figure 2 demonstrates the appearance of recycled CA and particle size distribution corresponding to the recycled CA along with FA.

Mix Design and Sample Preparation

The HFRGPC were prepared with PF added to the mortar mix at a volume fraction of 0.5%, 1%, and 1.5% of the total mixture volume and constant volume fraction of 1% for SF. A plain mix without any fiber was also produced for the purposes of comparison. The mix proportions are shown in Table 2. For preparing the sodium hydroxide solution with a molarity of 14 M, the NaOH flakes were weighed and then dissolved in distilled water 24 h before casting and kept in room temperature conditions to eliminate the rapid setting of the geopolymeric specimens due to excessive heat evolved. The sodium silicate solution was then added to the sodium hydroxide solution. The mixes were prepared with an alkaline ratio of 2.0 with a liquid–binder ratio of 0.475 and NaOH concentration of 14 M. At the beginning SCMs and FA were mixed first to have homogeneity. Recycled CA of desired size and quantity was prepared separately. Prepared dry mix of SCMs-FA was mixed with recycled CA and thoroughly mixed for three minutes. Subsequently, the aggregates and fibers were added to the mix together with the extra water. The mixing process was continued until a homogenous mix was achieved. It was necessary to add the fibers to the mix gradually to avoid agglomeration. Next, the fresh mixture was poured into the molds with the dimensions of 100 × 100 × 100 mm (cubic specimens) and 300 × 150 mm (cylindrical specimens) and vibrated for 15 s. The specimens were kept at a temperature of 23 °C for one day. After removing them from the mold, they were cured with temperature of 60 ± 5 °C in oven for 7 and 28 days (Table 3).

Heating Procedure

A day before conducting the tests, the specimens were heated to target temperatures of 200 °C, 400 °C, and 800 °C. This was achieved using an electric oven which had a temperature increase from ambient to the target temperature at a rate of 10 °C/min until the target elevated temperature was reached (200 °C, 400 °C, and 800 °C). The target temperature was maintained constant for three hours to ensure uniform heat distribution within the specimens. The specimens were then left to cool gradually until they reached the room temperature conditions of 25 °C under air cooling. The next day, the specimens were tested after taking the required measurements (Figure 3).

Testing Procedures

By investigating the mechanical characteristics of HFRGPC, the current study examination has assessed the effects of adding PF and SCMs, NZ and MK, by partly substituting Faah in geopolymer mixtures exposed to elevated temperature. Fresh properties of HFRGPC were determined in term of workability using the slump test according to ASTM C1611 [29]. Compressive strength tests on 100×100×100 cube specimens were executed according to ASTM C39 [33]. Splitting tensile strength tests were done on 150×300 mm cylinder specimens in accordance with ASTM C496 [34]. All tests were carried out in triplicate and average values were obtained and used as the results. Figure 4 demonstrates the preparation and testing of HFRGPC specimens.

Artificial Neural Network

Influenced by the biological neural structures present in animal brains, the principles of the artificial neural network (ANN) were initially introduced as a means to resolve a diverse range of intricate issues in the preceding century [36]. The architecture of an Artificial Neural Network (ANN) comprises of three layers, namely, the input layer, hidden layer, and output layer. The input layer accommodates a minimum of one input element, and the data in this layer produce an unprocessed output. The hidden layer is where the inputs undergo specific operations, and its structure and function may vary according to the network structure selection. It can be single-layered or multi-layered. The output layer contains a minimum of one output, and its value is dependent on the network function. This layer executes the process and transmits its output to the extrinsic environment (Lee et al. 2019; Meng et al. 2019; Nematzadeh et al. 2021). This particular model has the capability to encompass various basis functions for the concealed layer. In the context of regression problems, a linear function is deemed appropriate for the output layer. It is noteworthy that the regression function, which is approximated by an artificial neural network, can be expressed in a uniform manner, irrespective of the specific hidden basis function employed (Guijo-Rubio et al. 2020):

$$f(x, W, \beta) = \beta_0 + \sum_{j=1}^{m} \beta_j B_j(x, w_j) \tag{1}$$

Where $B_j(x, w_j)$ stands for the set of non-linear transformations of the input vector $x^T = (x_1, x_2, \dots, x_d)$, where $x^T \in R^d$; a bias term, β_0, is considered; $\beta^T = (\beta_1, \beta_2, \dots, \beta_m)$ are the coefficients from the hidden layer to the output layer; $W^T = (W_{j1}, W_{j2}, \dots, W_{jd})$ are the parameters from the input layer to the j-the hidden node, and finally, m is the number of basis functions or hidden neurons of the model. Through utilization of predetermined weight values during the process cycle, the training gradually evolves. This evolution is measured by comparing the predicted output with the recognized output, and subsequently redistributing error values in an attempt to determine proper weights and minimize the final error. Additionally, a pre-established parameter may be employed as the model and pattern threshold. Finally, a nominal amount of bias may be added to the input data result to determine the decision-making boundary and pattern threshold. The selection of the activation function is contingent upon the complexity of the issue at hand. For most nonlinear problems, Sigmoid functions, such as log-sigmoid or tangent sigmoid, may be implemented.

M5p Model Tree

By developing a binary decision tree and employing several linear regression functions at the leaf (terminal) nodes, Quinlan indicated his M5p model tree (M5p-MT) (Quinlan 1987). In the first phase, the supposed node's error level is considered the standard deviation of the class values for that node. Next, each attribute's expected decrease in error is calculated (Quinlan 1987). The term "Standard Deviation Reduction" (SDR) is used to define the reduction in errors:

$$SDR = sd(T) - \sum \frac{|T_i|}{T} sd(T_i) \tag{2}$$

In the equation above, sd stands for standard deviation, T_i for the number of samples that indicate the ith sample that might increase, and T for the overall sample number. Due to the splitting process, a child node's standard deviation is lower than a parent node's. The optimal split is ultimately selected after assessing all feasible divides in sequence.

Evaluation Criteria

In the present study, the proposed models were assessed by means of various performance measures (Eqs. (3)-(6)). The measures of precision and error employed in this study encompassed the correlation coefficient (R), root mean square error (RMSE), mean absolute error (MAE), and uncertainty at 95% (U95). These metrics were expressed as follows.

$$R = \frac{\sum_{i=1}^{N}(T_{obs}-\overline{T_{obs}}).(T_{pre}-\overline{T_{pre}})}{\sqrt{\sum_{i=1}^{N}(T_{obs}-\overline{T_{obs}})^2 \sum_{i=1}^{N}(T_{pre}-\overline{T_{pre}})^2}} \tag{3}$$

$$RMSE = \sqrt{\frac{1}{N}\sum_{i=1}^{N}\left(T_{pre}-T_{obs}\right)^2} \tag{4}$$

$$MAE = \frac{\sum_{i=1}^{N}\left|T_{pre}-T_{obs}\right|}{\mathrm{N}} \tag{5}$$

$$U_{95} = 1.96\sqrt{(\mathrm{STDEV}^2 + \mathrm{RMSE}^2)} \tag{6}$$

Where T_{obs} and T_{pre} are the observed and predicted values, respectively; $\overline{T_{obs}}$ and $\overline{T_{pre}}$ represent the mean of the observed and predicted values, respectively; and N is the number of data.

RESULTS AND DISCUSSION

Workability

The slump of different concrete mixture tested in this study is shown in Figure 5. When MK was replaced with FAsh in HFRGPC, the related slump was decreased. This is because that the fly ash (Kurda etal. 2017) acted as lubricant and increased the workability of concrete. Hasnaoui et al. (2019) concluded that the GPC based on MK decrease the workability due to increase the MK/activator ratio and their high-water demand which led to increasing the flow time. Additionally, the results provided in Figure 5 show that zeolite used to replace FAsh has increases the slump of HFRGPC. The slump of the mixtures containing zeolite is mainly influenced by the porous structure of the zeolite and high specific surface area of zeolite particles, resulting in high absorption rate and thus reduced amount of free water (Azarijafari et al. 2014).

It can be observed from the figure that the slump of HFRGPC decreases continuously with the increase of polypropylene fibre content. As the PF content increases, the friction in the material continues to increase, which inhibits the flow of the material, and the fibre itself can also act as a bridge to prevent the material from slipping.

Compressive Strength

The addition of different pozzolans to the HFRGPC matrix has provided different results for compressive strength. The use of metakaolin as a source of aluminosilicate in HFRGPC samples increased the compressive strength compared to samples containing FAsh. This may have been due to the higher calcium content of the metakaolin compared to FAsh. Higher calcium content in the source of aluminosilicate increased the possibility of Ca-Al-Si formation in the microstructure, which strengthened the mechanical properties of the HFRGPC (Kumar et al. 2010; Hadi et al. 2017). According to Figure 6, it can be observed that the 10% and 20% MK replacements increased the compressive strength at 28 days by about 12.6% and 24.2% compared with the control mix in a group with 0% PF, which agreed with Duan et al. (2016), and Nuaklong et al. (2018).

In addition, the compressive strength of HFRGPC with constant MK replacement (i.e. 10%) is measured about 36.54 and 31.8 MPa, respectively, when NZ is replaced with FAsh by 10 and 20%. The aforementioned observation is consistent with prior research results regarding the compressive strength of GPC that incorporates NZ. According to previous studies, the escalation of NZ concentration within the concrete mixes is likely to induce the creation of cavities, voids, and uneven morphological features. As a result, the mechanical properties of the concrete are diminished (Ahdal et al. 2022). However, the results also demonstrated that after seven days, the compressive strength of the specimens increased even by the addition of zeolite, so that the specimen with 10 wt% of FAsh replaced by zeolite showed almost equal or higher strength at 28 days of curing, compared to the specimen containing 10% MK. This can be due to the low reactivity of zeolite at early age and helping to form strengthening phases at older age.

Moreover, the inclusion of PF increased the compressive strength of HFRGPC substantially, and these characteristics were further improved by increasing the PF volume. The primary reason that PF improves the compressive behavior of HFRGPC is that they act as a bridging agent (Qaidi et al. 2022), forming a high core strength inside the concrete specimen during compression and preventing lateral-expansion. When a sample is compressed, a lateral-expansion happens in the center of the sample's height. The bridging function of PF enhanced the cohesiveness between the concrete aggregates and paste and the tensile strength of the concrete matrix (Wang et al. 2020; Tayeh et al. 2022), which limits lateral-expansion and therefore improves the compressive behavior of PF-reinforced GPC. As a result, although the addition of fibers did not have much effect on the compressive strength of the geopolymer specimens, the maximum compressive strength value was reached when 1 % PF was introduced.

Modulus of Elasticity

Studies have shown that the modulus of elasticity of GPC was lower than that of ordinary concrete (Hardjito and Rangan 2005; Sofi et al. 2007; Nath and Sarker 2017; Hassan et al. 2019; Fernández-Jiménez et al. 2003) and generally, the value of elasticity varied with the compressive strength. This is also true for HFRGPC. It has been shown that in RefGPC without fibers, the modulus of elasticity of the HFRGPC was 23.7 GPa while with the use of 0.5%, 1%, and 1.5% PF, the modulus of elasticity of the HFRGPC was 23.9, 25.1, and 22.1 GPa, respectively (Figure 7). By incorporating MK as the 10 and 20% replacement of FAsh, increased the modulus of elasticity, respectively, about 6% and 27% for all groups of HFRGPC. Similar to compressive strength, addition of PF up to 1% gradually improved the modulus of elasticity of HFRGPC and greater inclusion of PF will reduce this characteristic accordingly. For example, modulus of elasticity of M20Z10 specimen containing 0.5, 1, and 1.5% PF changed by 0.34, 1.7, and -7.5%, respectively, compared to RefGPC.

The test results are compared with the modulus of elasticity predicted by the equations given in CEB-FIB model code and that proposed by Hardjito et al. (2004), Lee and Lee (2013), and Nath and Sarker (2016) as described below.

$$E_{CEB-FIB} = 0.85 \times 2.15 \times 10^4 \times (\frac{f_c}{10})^{1/3} \quad (7)$$

$$E_{Hardjito\ et\ al} = 2707\sqrt{f_c} + 5300 \quad (8)$$

$$E_{Lee\ and\ Lee} = 5300\sqrt[3]{f_c} \quad (9)$$

$$E_{Nath\ and\ Sarker} = 3.51\sqrt{f_c} \quad (10)$$

Where E is the modulus of elasticity of concrete (GPa) and f_c is the average compressive strength (MPa). The values of modulus of elasticity are plotted in Figure 8 and compared with the values predicted by the above equations. It is clear that, the experimental values of modulus of elasticity of HFRGPC are upper than those calculated according to recommended equations of Hardjito et al., Lee and Lee, and Nath and Sarker, except CEB-FIB code model. Comparing with the model equations for GPC, it can be seen that the model provided by Nath and Sarker (2016) fits most with the results of this study, whereas the model by Lee and Lee (2013) predicts lower values than experimental values. This is possibly due to the variation of the types of fly ash, different mixture compositions and curing condition used in those respective studies.

The experimental values have been analysed to fit in a general equation using commonly used term, square root of compressive strength ($\sqrt{f_c}$). A regression analysis by the method of least square was performed to fit the data in a given equation. The analysis proposed the final equation as follows:

$$\mathrm{E} = 5.672\sqrt{\mathrm{f_c}} - 10.038 \quad (11)$$

Values calculated with Eq. (15) are also plotted in Figure 7. It can be seen that Eq. (8) from regression analysis matches very well with the experimental results. Hence Eq. (8) is proposed for predicting the modulus of elasticity of HFRGPC.

Splitting Tensile Strength

Figure 9 shows the splitting tensile strength test results for HFRGPC samples at the test age of 7 and 28 days. The tensile strength increases by increasing replacement ratio up to 50% then decreases with a very slow rate. The results show a similar general trend to the compressive strength results, i.e. improved strength values compared to the RefGPC specimen and optimal results at 1% PF content. However, the presence of PF indicates a much greater effect on the tensile strength compared to compressive strength. In this regard, the 1% HFRGPC (M20) showed the highest tensile strength (28-day strength equal to 5.7 MPa) among all HFRGPC; around 54% increase compared to the RefGPC specimen without PF. Previous studies on the tensile strength of fibre-reinforced GPCs too showed beneficial effects from polymeric fibres.

The advantageous effect of fibres on tensile strength of GPC leads to enhanced ductility characteristics over plain (no fiber) GPC. The polymeric fibers improve the geopolymeric matrix of the composites in terms of formation and/or redistribution of cracks by bridging cracks and perforations within the matrix (Hasnaoui et al. 1998).

The relation between splitting tensile strength and compressive strength of HFRGPC containing different percentages of PF was plotted and shown in Figure 10. According to R^2, correlation between compressive strength and splitting tensile strength for HFRGPC containing 0, 0.5, and 1% is about 95% and can be stated that the predicted error of splitting tensile strength approximately runs below 5% for the HFRGPC with up to 1% PF. However, the predicted error is significant, about 22%, for the HFRGPC with 1.5% PF and R^2 for this group of HFRGPC is calculated 0.76.

Effect of Temperature on the Compressive Strength

The compressive strength results and relative values of the heated and unheated test HFRGPC containing 1% PF after 28 days are shown in Figure 11. Three samples per batch were tested and the average strength has been accordingly reported. At the age of 28 days, the specimens were heated in an electric furnace at 200 °C, 400 °C, and 700 °C. According to the test results, since the samples of HFRGPC were exposed to heating, it has been observed that the compressive strength increased till 400 °C for all samples. The compressive strength of P1-M20 at 400 °C increased about 7% and 13%, respectively, compared to HFRGPC specimens exposed to 200 and 23 °C. A similar behaviour is also observed in P1-M20Z10 with slightly higher increment of about 15% at 23 °C and 9% at 200 °C. With further increase in temperature at 700 °C the compressive strength of HFRGPC specimens decreased by about 44, 40, 38%, respectively, compared to those at 400, 200, and 23 °C which is also reported by Chen and Liu [1]. The P1-M10 and P1-M20 maintained the residual compressive strengths of 25.2 and 32.64 MPa at 700 °C, respectively and thus recording a minimum strength loss of 40 and 38%, respectively (Table 4).
This behaviour was attributed to the formation of discontinuous nano-pores and dehydration shrinkage of geopolymers due to expel of free water at 400 °C (Kurda et al. 2017). Nevertheless, with further increase in elevated temperature at 700 °C, all samples showed deterioration in compression strength. This phenomenon resulted due to the thermal incompatibility (i.e. differential thermal expansion between geopolymer and basalt microfibrils), pore pressure effects (i.e. movement of free water and hydroxyls) and possible phase transition in geopolymers (Quinlan 1987; Rickard et al. 2013). At elevated temperature exposure, several events such as evaporation of water adsorbed by N-A-S-H gel, formation of anhydrous products, crystallization of stable anhydrous phases and melting (sintering) occurred, which subsequently deteriorated the mechanical properties (Rickard et al. 2013).

Scanning Electron Microscopy (SEM)

SEM analysis was conducted to investigate the microstructural changes of the HFRGPC reinforced with 1% PF (P1-M20), which exhibited superior fire resistance performance at different temperatures among different percentages of MK and NZ as the replacement of FAsh in HFRGPC mixtures. Figure 12 shows the SEM images of the HFRGPC after exposure to temperatures of 23 200, 400, and 700 °C. For unheated specimens (23 °C), some micro-cracks were detected in the compact microstructure and C-A-S-H gel. The cracks were probably formed due to the drying shrinkage, which is typical for GPC composites.
As can be observed in Figure 12, the exposure to elevated temperatures caused a considerable transformation in the microstructures of GPC. At 200 °C, a few distinctive black areas, which signals the formation of pores and cavities and some marked micro-cracks for the specimen were observed. Such voids can be formed due to the moisture loss and contraction of paste. Still, the C-A-S-H gel was not decomposed and the hydration products remained nearly intact. Furthermore, no sign of debonding at the fibre–matrix interface was noticed. It indicated that the exposure to 200 °C did not affect the fibre–matrix bond negatively and some extra crystals of C-A-S-H were formed in the matrix, which justified the strength gain of mixes at 200 °C compared to the ambient temperature. At 400 and 700 °C, micro-cracks and voids in the matrix were expanded, which is due mainly to the decomposition of C-A-S-H gels, loss of crystal water, and mismatch in the thermal expansion rates of paste and aggregates which is stated in (Behfarnia and Shahbaz 2018). Also, it was observed that some aggregates were detached from the paste and the fibre–matrix bond was weakened. At such high temperatures, the thermally-induced cracks due to the thermal gradient in the mix became more significant (Rashad et al. 2016; Shoaei et al. 2021). Furthermore, as the temperature was increased, the number of micro-cracks and gaps in the matrix was increased as well, which is probably owing to the melting of fibres.

Statistical Analysis

Machine Learning (ML) Models

In the present investigation, the employment of ANN methodology was executed, wherein five neurons for FAsh, MK, NZ, PF, and temperature (T) in the input layer and one neuron for compressive strength in the output layer were taken into account and governed by a linear function. The determination of the quantity of neurons in the hidden layers was accomplished by means of a trial and error technique, which commenced with a single neuron and progressed up to a maximum of ten neurons. Furthermore, the optimal configuration for model development was subsequently determined by adopting the most effective arrangement. The final structure of the ANN for predicting compressive strength involved the use of a single hidden layer containing three neurons. In order to minimize the error for these neurons, the back-propagation algorithm was employed in conjunction with a feedforward approach and an adaptive learning rate of 0.3, a momentum rate of 0.2, and a learning cycle of 2000. The efficacy of various trained models was compared, and ultimately the most precise model was determined.

The M5p-MT technique for the compressive strength prediction of the HFRGPC utilized WEKA 3.7 software. In the present section, an assessment is made of the capacity of the M5p-MT approach in relation to identifying the mathematical expression of linear equations in relation to compressive strength. The initial parameters of the M5p-MT technique were set at their default values, namely, a pruning factor of 5.0 and the application of a smoothing option. After classifying, this model including five inputs and one output parameters was implemented for the compressive strength of HFRGPC prediction using 6 rules that is presented in Table 5.

Evaluation results of the compressive strength prediction of the HFRGPC using ANN and M5p-MT techniques performing performance metrics are shown in Table 6. From the results, it can be seen that the accuracy of both machine learning models in the prediction of the compressive strength is likely similar for training stage. However, the difference in the performance of ML models is clearly can be observed in testing stage and comparing the error criteria such as RMSE and MAE indicated that M5p-MT models had lower error than ANN model by about 5.63 and 6.58% for testing stage. To furnish further elaboration on the outcomes and to ascertain the model's variance with regards to anticipations of compressive strength, the U95 has been determined. It is noteworthy that the coverage factor of 1.96 corresponds to the 95% confidence level of anticipated values of the models. Therefore, the M5p-MT model registers a lower value of U95, of approximately 25.29% and 21.17% during the training and testing stages, respectively, whereas this metric is calculated about 26.91% and 23.74% for ANN model in the prediction of compressive strength of HFRGPC.

The degree of agreement between experimental and predicted compressive strength of HFRGPC at training and testing stages was visually evaluated using scatterplots (Figure 13a). The analysis revealed a very good simulation performance for the compressive strength of the HFRGPC using ANN and M5p-MT models at training and testing stages. In addition, for displaying the prediction result and changes in a set of experimental compressive strength, especially for extreme values, line graph is depicted in Figure 13b. According to this figure, it can be seen that M5p-MT model is nearer than ANN model to the experimental results and its relative error (RE) exhibits a lower limit compared to ANN model in the prediction of compressive strength of HFRGPC.

Analysis of Variance (ANOVA)

In this section, the contribution of parameters influencing the compressive strength of HFRGPC including percentage of MK and NZ replacement, PF, and T was evaluated. For this purpose, analysis of variance (ANOVA) method was employed, which is a powerful statistical tool to calculate the contribution of the input parameters to the response of a system and it has been widely applied to different engineering problems [54,55]. ANOVA was performed on the results of compressive strength test of HFRGPC by considering MK, NZ, PF, and T as the variables. The detailed results of the analysis are presented in Table 7. In this table, DF, SS, and Var respectively represent degrees of freedom, sum of square, and variance of each variable. In addition, p-value is used for statistical hypothesis testing and as given in Table 7, it was smaller than 0.05 in all cases, which indicated that the input parameters significantly influenced the compressive strength. The results show that temperature has a major influence on the compressive strength of HFRGPC, with percent contributions of 71.98% and the lowest contribution related to NZ with 5.52%.

CONCLUSIONS

In this paper, the experimental performance of HFRGPC was evaluated in workability, compressive strength, modulus of elasticity, and splitting tensile strength tests at various PF volume fractions, and the fire resistance of the HFRGPC mixes with the optimum percentage of PF is investigated. Based on the experiment results, the following conclusions were drawn:

(1) The addition of MK into the HFRGPC as the replacement of FAsh affected the slump of the HFRGPC mixes adversely, whereas NZ replacement due to its high specific surface area and the porous structure increases workability. In addition, by increasing the PF inclusion, the slump of HFRGPC decreases continuously.

(2) The optimum PF content for achieving the maximum compressive strength (52.7 MPa), modules of elasticity (30.6 GPa), and splitting tensile strength (5.7 MPa) is determined 1% for HFRGPC mixes containing 20% MK substitution.

(3) All HFRGPC mixes show an increase of about 10–15% in compressive strength when exposed to 200 °C, and the increment rises up to 400 °C of exposure. With further increase in temperature at 700 °C the compressive strength of all HFRGPC specimens deteriorated and decreased by about 40%. The P1-M10 and P1-M20 maintained the residual compressive strengths of 25.2 and 32.64 MPa at 700 °C, respectively and thus recording a minimum strength loss of 40 and 38%, respectively.

(4) The prediction results of ML techniques indicated an accurate and validated simulation through the experimental compressive strength values in both training and testing stages in term of correlation coefficient. However, the difference in the performance of ML models is clearly can be observed in terms of RMSE and MAE and the proposed formula by M5p-MT models had lower error than ANN model by about 5.63 and 6.58% for testing stage.
(5) The results of ANOVA also show that temperature has a major influence on the compressive strength of HFRGPC, with percent contributions of 71.98% and the lowest contribution related to NZ with 5.52%.

DATA AVAILABILITY STATEMENT:
Some or all data, models, or code that support the findings of this study are available from the corresponding author upon reasonable request.

REFERENCES:
1. Abdollahnejad, Z., Mastali, M., Falah, M., Shaad, K. M., Luukkonen, T., and Illikainen, M. 2021. “Durability of the Reinforced One-Part Alkali-Activated Slag Mortars with Different Fibers.” Waste and Biomass Valorization, 12 (1), 487–501.
2. Ahdal, A. Q., Amrani, M. A., Ghaleb, A. A. A., Abadel, A. A., Alghamdi, H., Alamri, M., et al. 2022. “Mechanical performance and feasibility analysis of green concrete prepared with local natural zeolite and waste PET plastic fibers as cement replacements.” Case Studies in Construction Materials, 17, e01256.
3. Albidah, A., Alghannam, M., Abbas, H., Almusallam, T., and Al-Salloum, Y. 2021. “Characteristics of metakaolin-based geopolymer concrete for different mix design parameters.” Journal of Materials Research and Technology, 10, 84–98.
4. Amran, Y. H. M., Alyousef, R., Alabduljabbar, H., and El-Zeadani, M. 2020. “Clean production and properties of geopolymer concrete; A review.” Journal of Cleaner Production, 251, 119679.
5. Anna, J. J. M., and Sumathi, A. 2018. “Strength and durability characteristics of steel fibre reinforced geopolymer concrete.” Int. J. Eng. Technol., 7 (3.12), 337.
6. Aslani, F., and Kelin, J. 2018. “Assessment and development of high-performance fibre-reinforced lightweight self-compacting concrete including recycled crumb rubber aggregates exposed to elevated temperatures.” Journal of Cleaner Production, 200, 1009–1025.
7. Awolusi, T. F., Oke, O. L., Akinkurolere, O. O., and Sojobi, A. O. 2019. “Application of response surface methodology: Predicting and optimizing the properties of concrete containing steel fibre extracted from waste tires with limestone powder as filler.” Case Studies in Construction Materials, 10, e00212.
8. Aydin, S., and Baradan, B. 2013. “The effect of fiber properties on high performance alkali-activated slag/silica fume mortars.” Composites Part B: Engineering, 45 (1), 63–69.
9. Azarijafari, H., Kazemian, A., Ahmadi, B., Berenjian, J., and Shekarchi, M. 2014. “Studying effects of chemical admixtures on the workability retention of zeolitic Portland cement mortar.” Construction and Building Materials, 72, 262–269.
10. Behfarnia, K., and Shahbaz, M. 2018. “The effect of elevated temperature on the residual tensile strength and physical properties of the alkali-activated slag concrete.” Journal of Building Engineering, 20, 442–454.
11. Bhogayata, A., Dave, S. V., and Arora, N. K. 2020. “Utilization of expanded clay aggregates in sustainable lightweight geopolymer concrete.” Journal of Material Cycles and Waste Management, 22 (6), 1780–1792.
12. Chen, K., Wu, D., Xia, L., Cai, Q., and Zhang, Z. 2021. “Geopolymer concrete durability subjected to aggressive environments – A review of influence factors and comparison with ordinary Portland cement.” Construction and Building Materials, 279, 122496.
13. Choi, J., Lee, B. Y., Ranade, R., Li, V. C., and Lee, Y. 2016. “Ultra-high-ductile behavior of a polyethylene fiber-reinforced alkali-activated slag-based composite.” Cement and Concrete Composites, 70, 153–158.
14. Deb, P. S., Nath, P., and Sarker, P. K. 2014. “The effects of ground granulated blast-furnace slag blending with fly ash and activator content on the workability and strength properties of geopolymer concrete cured at ambient temperature.” Materials and Design, 62, 32–39.
15. Dias, D. P., and Thaumaturgo, C. 2005. “Fracture toughness of geopolymeric concretes reinforced with basalt fibers.” Cement and Concrete Composites, 27 (1), 49–54.
16. Duan, P., Yan, C., and Zhou, W. 2016. “Influence of partial replacement of fly ash by metakaolin on mechanical properties and microstructure of fly ash geopolymer paste exposed to sulfate attack.” Ceramics International, 42 (2), 3504–3517.
17. Elsheikh, A. H., Sharshir, S. W., Abd Elaziz, M., Kabeel, A. E., Guilan, W., and Haiou, Z. 2019. “Modeling of solar energy systems using artificial neural network: A comprehensive review.” Solar Energy, 180, 622–639.

18. Environment, U. N., Scrivener, K. L., John, V. M., and Gartner, E. M. 2018. "Eco-efficient cements: Potential economically viable solutions for a low-CO2 cement-based materials industry." Cement and Concrete Research, 114, 2–26.
19. Erfanimanesh, A., and Sharbatdar, M. K. 2020. "Mechanical and microstructural characteristics of geopolymer paste, mortar, and concrete containing local zeolite and slag activated by sodium carbonate." Journal of Building Engineering, 32, 101781.
20. Guijo-Rubio, D., Durán-Rosal, A. M., Gutiérrez, P. A., Gómez-Orellana, A. M., Casanova-Mateo, C., Sanz-Justo, J., et al. 2020. "Evolutionary artificial neural networks for accurate solar radiation prediction." Energy, 210, 118374.
21. Gülşan, M. E., Alzeebaree, R., Rasheed, A. A., Niş, A., and Kurtoğlu, A. E. 2019. "Development of fly ash/slag based self-compacting geopolymer concrete using nano-silica and steel fiber." Construction and Building Materials, 211, 271–283.
22. Hadi, M. N. S., Farhan, N. A., and Sheikh, M. N. 2017. "Design of geopolymer concrete with GGBFS at ambient curing condition using Taguchi method." Construction and Building Materials, 140, 424–431.
23. Hasnaoui, A., Ghorbel, E., and Wardeh, G. 2019. "Optimization approach of granulated blast furnace slag and metakaolin based geopolymer mortars." Construction and Building Materials, 198, 10–26.
24. Jindal, B. B., Alomayri, T., Hasan, A., and Kaze, C. R. 2023. "Geopolymer concrete with metakaolin for sustainability: a comprehensive review on raw material's properties, synthesis, performance, and potential application." Environmental Science and Pollution Research, 30 (10), 25299–25324.
25. Kumar, S., Kumar, R., and Mehrotra, S. P. 2010. "Influence of granulated blast furnace slag on the reaction, structure and properties of fly ash based geopolymer." Journal of Materials Science, 45 (3), 607–615.
26. Kurda, R., de Brito, J., and Silvestre, J. D. 2017. "Influence of recycled aggregates and high contents of fly ash on concrete fresh properties." Cement and Concrete Composites, 84, 198–213.
27. Lee, Y., Choi, J., and Kim, H. K. 2017. "Effects of a defoamer on the compressive strength and tensile behavior of alkali-activated slag-based cementless composite reinforced by polyethylene fiber." Composite Structures, 172, 166–172.
28. Lee, S., Lee, K. K., and Yoon, H. 2019. "Using artificial neural network models for groundwater level forecasting and assessment of the relative impacts of influencing factors." Hydrogeology Journal, 27 (2), 567–579.
29. Mahmoodi, O., Siad, H., Lachemi, M., Dadsetan, S., and Sahmaran, M. 2021. "Development and characterization of binary recycled ceramic tile and brick wastes-based geopolymers at ambient and high temperatures." Construction and Building Materials, 301, 124138.
30. Mastali, M., Alzaza, A., Mohammad Shaad, K., Kinnunen, P., Abdollahnejad, Z., Woof, B., et al. 2019. "Using Carbonated BOF Slag Aggregates in Alkali-Activated Concretes." Materials, 12 (8), 1288.
31. Meng, E., Huang, S., Huang, Q., Fang, W., Wu, L., and Wang, L. 2019. "A robust method for non-stationary streamflow prediction based on improved EMD-SVM model." Journal of Hydrology, 568, 462–478.
32. Nematzadeh, M., Shahmansouri, A. A., and Zabihi, R. 2021. "Innovative models for predicting post-fire bond behavior of steel rebar embedded in steel fiber reinforced rubberized concrete using soft computing methods." Structures, 31, 1141–1162.
33. Nuaklong, P., Sata, V., and Chindaprasirt, P. 2018. "Properties of metakaolin-high calcium fly ash geopolymer concrete containing recycled aggregate from crushed concrete specimens." Construction and Building Materials, 161, 365–373.
34. Patil, S. S. and Patil, A. A. 2015. "Properties of polypropylene fiber reinforced geopolymer concrete." Int. J. Curr. Eng. Technol., 5 (4), 29092912.
35. Pradhan, P., Dwibedy, S., Pradhan, M., Panda, S., and Panigrahi, S. K. 2022. "Durability characteristics of geopolymer concrete - Progress and perspectives." Journal of Building Engineering, 59, 105100.
36. Qaidi, S. M. A., Sulaiman Atrushi, D., Mohammed, A. S., Unis Ahmed, H., Faraj, R. H., Emad, W., et al. 2022. "Ultra-high-performance geopolymer concrete: A review." Construction and Building Materials, 346, 128495.
37. Quinlan, G. 1987. "Models of subsidence mechanisms in intracratonic basins, and their applicability to North American examples." Sedimentary Basins and Basin-Forming Mechanisms — Memoir, 12, 463-481.
38. Rajak, M., and Rai, B. 2019. "Effect of Micro Polypropylene Fibre on the Performance of Fly Ash-Based Geopolymer Concrete." Journal of Applied Engineering Sciences, 9 (1), 97–108.
39. Ranjbar, N., Talebian, S., Mehrali, M., Kuenzel, C., Cornelis Metselaar, H. S., and Jumaat, M. Z. 2016. "Mechanisms of interfacial bond in steel and polypropylene fiber reinforced geopolymer composites." Composites Science and Technology, 122, 73–81.

40. Rashad, A. M., Sadek, D. M., and Hassan, H. A. 2016. "An investigation on blast-furnace stag as fine aggregate in alkali-activated slag mortars subjected to elevated temperatures." Journal of Cleaner Production, 112, 1086–1096.
41. Rickard, W. D. A., Vickers, L., and van Riessen, A. 2013. "Performance of fibre reinforced, low density metakaolin geopolymers under simulated fire conditions." Applied Clay Science, 73 (1), 71–77.
42. Shaikh, F. U. A., and Hosan, A. 2016. "Mechanical properties of steel fibre reinforced geopolymer concretes at elevated temperatures." Construction and Building Materials, 114, 15–28.
43. Shehata, N., Sayed, E. T., and Abdelkareem, M. A. 2021. "Recent progress in environmentally friendly geopolymers: A review." Science of the Total Environment, 762, 143166.
44. Shoaei, P., Ghassemi, P., Ameri, F., Musaeei, H. R., Chee Ban, C., and Ozbakkaloglu, T. 2021. "Comparative study on the effect of fiber type and content on the fire resistance of alkali-activated slag composites." Construction and Building Materials, 288, 123136.
45. Singh, N. B., and Middendorf, B. 2020. "Geopolymers as an alternative to Portland cement: An overview." Construction and Building Materials, 237, 117455.
46. Suwan, T., Fan, M., and Braimah, N. 2016. "Micro-mechanisms and compressive strength of Geopolymer-Portland cementitious system under various curing temperatures." Materials Chemistry and Physics, 180, 219–225.
47. Tanyildizi, H., and Yonar, Y. 2016. "Mechanical properties of geopolymer concrete containing polyvinyl alcohol fiber exposed to high temperature." Construction and Building Materials, 126, 381–387.
48. Tayeh, B. A., Akeed, M. H., Qaidi, S., and Bakar, B. H. A. 2022. "Influence of microsilica and polypropylene fibers on the fresh and mechanical properties of ultra-high performance geopolymer concrete (UHP-GPC)." Case Studies in Construction Materials, 17, e01367.
49. Ting, M. Z. Y., Wong, K. S., Rahman, M. E., and Selowarajoo, M. 2021. "Prediction model for hardened state properties of silica fume and fly ash based seawater concrete incorporating silicomanganese slag." Journal of Building Engineering, 41, 102356.
50. Top, S., Vapur, H., Altiner, M., Kaya, D., and Ekicibil, A. 2020. "Properties of fly ash-based lightweight geopolymer concrete prepared using pumice and expanded perlite as aggregates." Journal of Molecular Structure, 1202, 127236.
51. Turner, L. K., and Collins, F. G. 2013. "Carbon dioxide equivalent (CO2-e) emissions: A comparison between geopolymer and OPC cement concrete." Construction and Building Materials, 43, 125–130.
52. Vilaplana, J. L., Baeza, F. J., Galao, O., Alcocel, E. G., Zornoza, E., and Garcés, P. 2016. "Mechanical properties of alkali activated blast furnace slag pastes reinforced with carbon fibers." Construction and Building Materials, 116, 63–71.
53. Wang, Y., Aslani, F., and Valizadeh, A. 2020. "An investigation into the mechanical behaviour of fibre-reinforced geopolymer concrete incorporating NiTi shape memory alloy, steel and polypropylene fibres." Construction and Building Materials, 259, 119765.
54. Wang, Z., Bai, E., Huang, H., Liu, C., and Wang, T. 2023. "Dynamic mechanical properties of carbon fiber reinforced geopolymer concrete at different ages." Ceramics International, 49(1), 834–846.
55. Zanotti, C., Borges, P. H. R., Bhutta, A., and Banthia, N. 2017. "Bond strength between concrete substrate and metakaolin geopolymer repair mortar: Effect of curing regime and PVA fiber reinforcement." Cement and Concrete Composites, 80, 307–316.

FIGURE CAPTION LIST:

Figure 1. X-ray diffraction (XRD) test for used pozzolans.

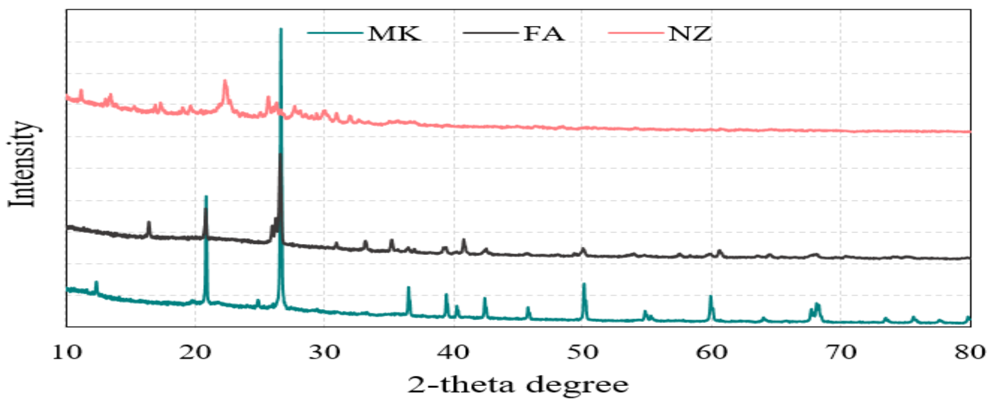

Figure 2. a) Appearance of Recycled CA; and b) Particle size distributions of recycled CA and FA used for GPC mixtures.

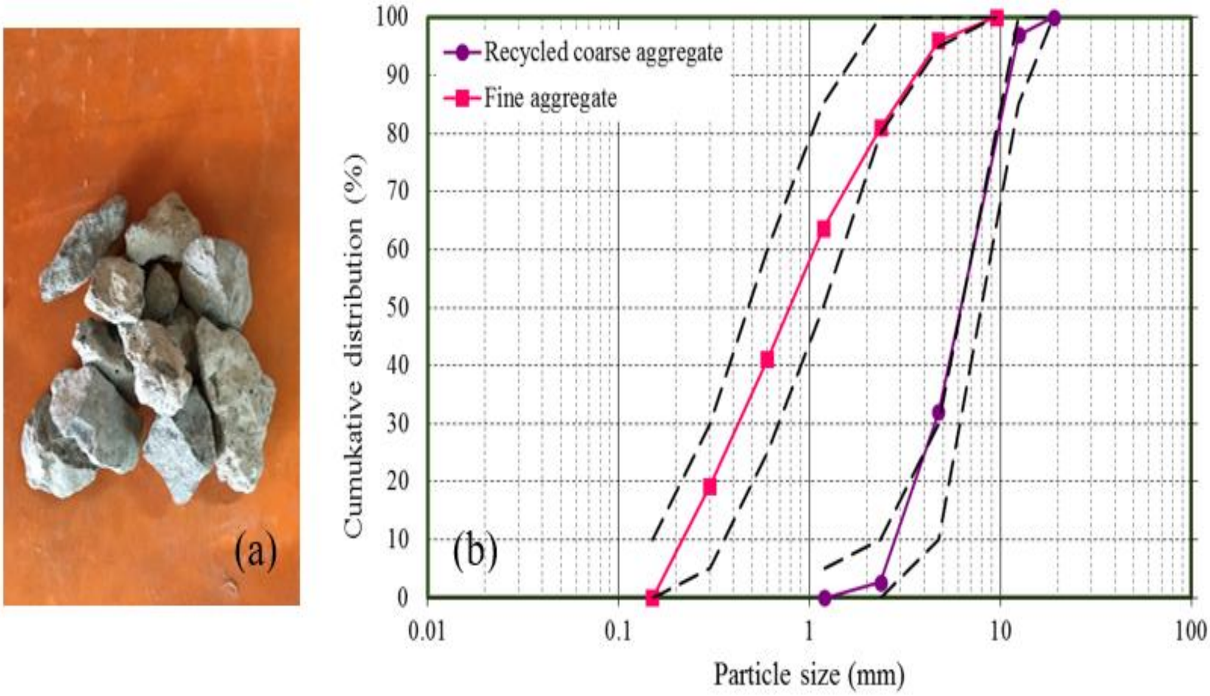

Figure 3. The heating regime inside the furnace.

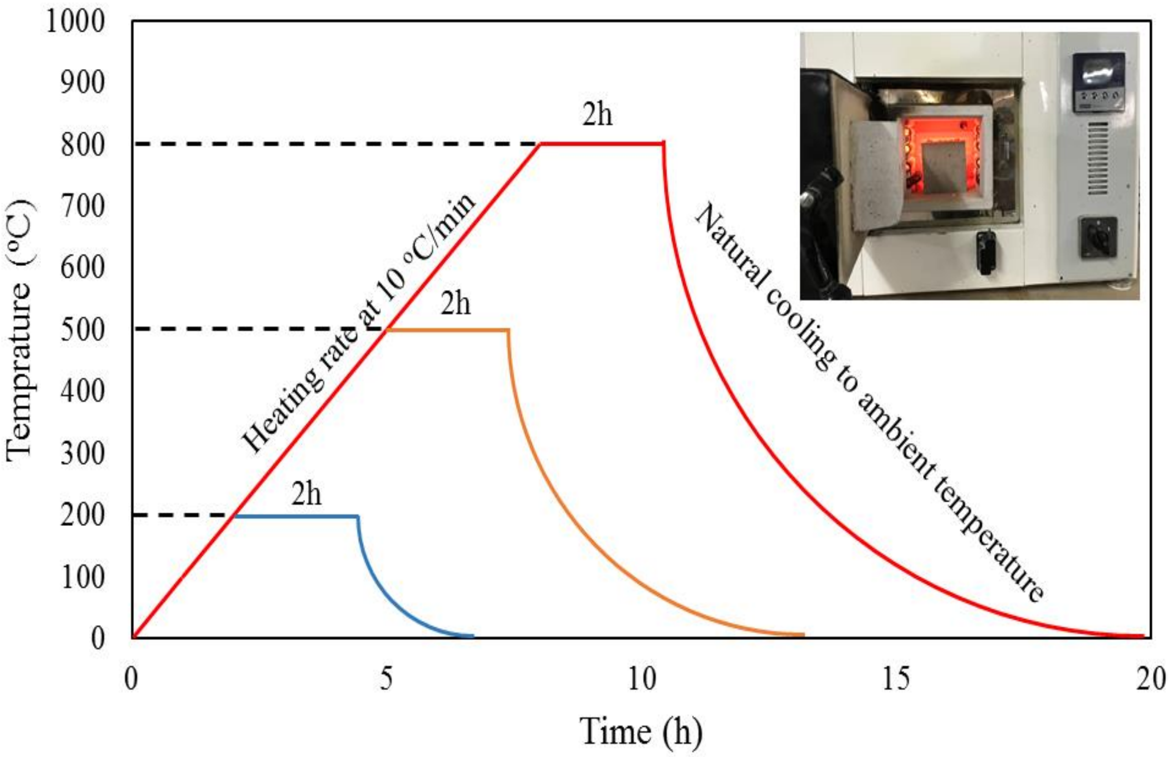

Figure 4. Preparation and testing of HFRGPC specimens.

Figure 5. Slump of different groups of concrete mixture. (The specimen names in the horizontal axis are listed in Table 3).

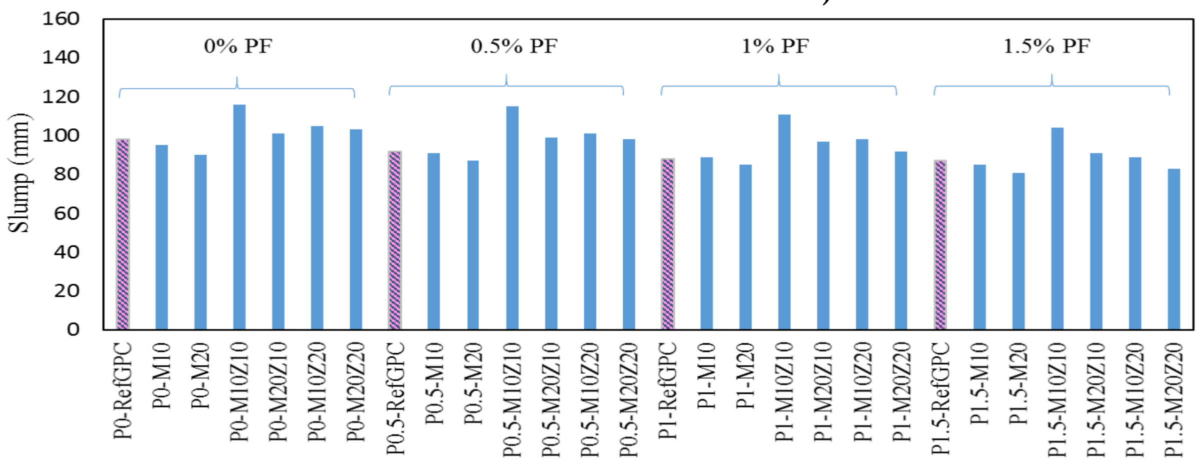

Figure 6. Compressive strength results of HFRGPC versus polypropylene fiber contents.

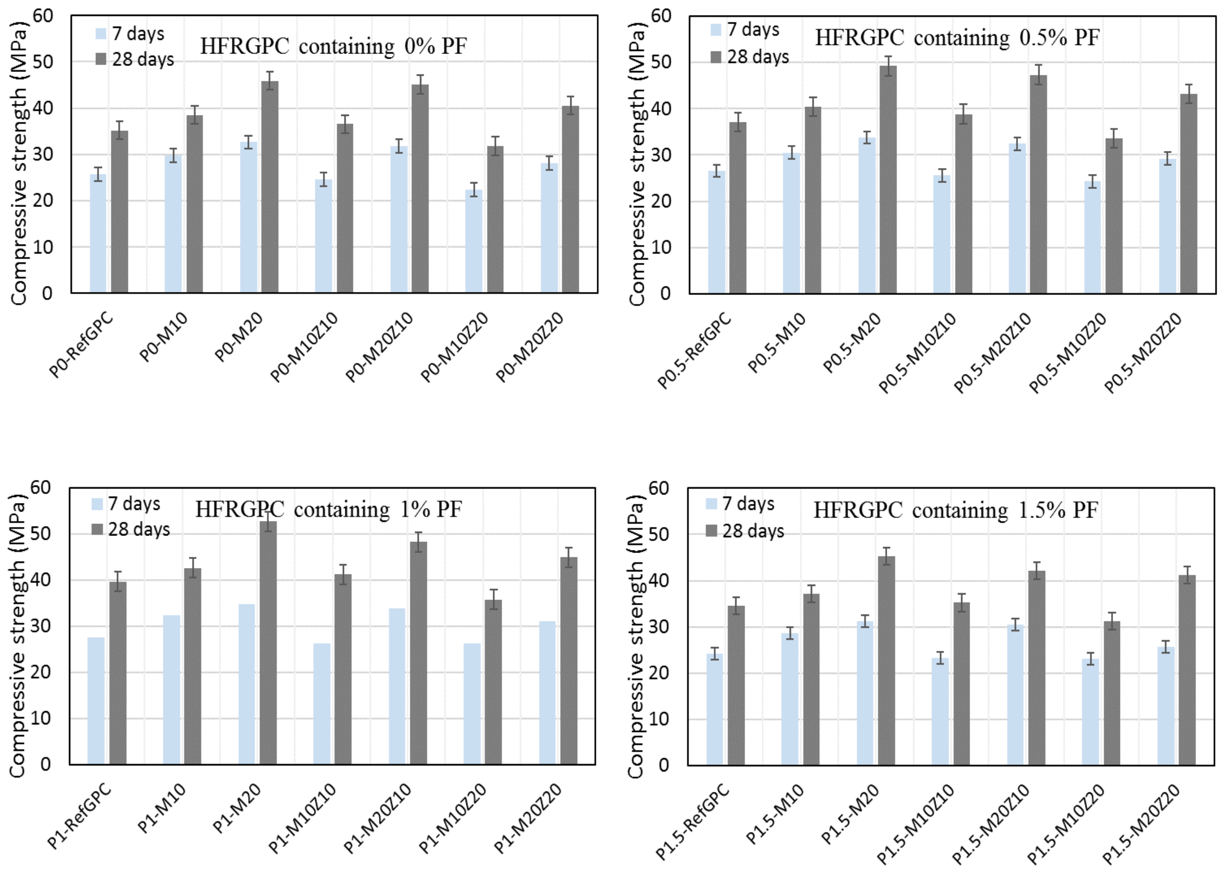

Figure 7. Modulus of elasticity results versus polypropylene fiber contents.

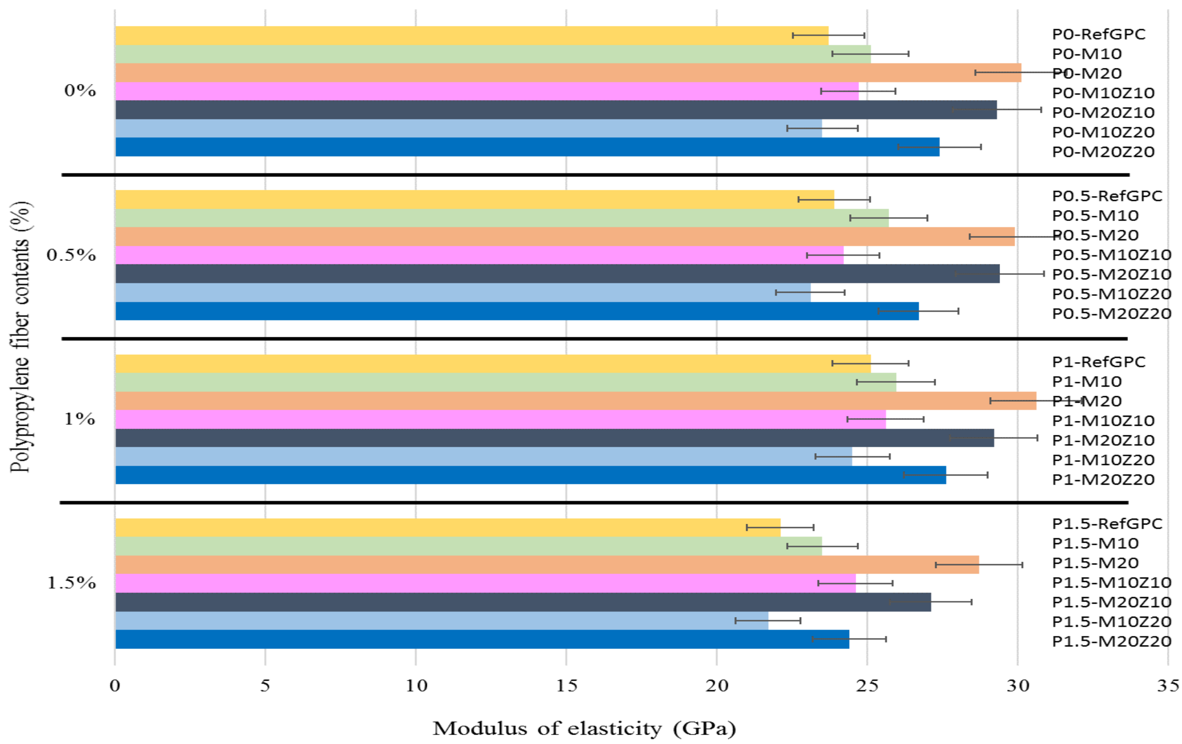

Figure 8. Relationship of modulus of elasticity with compressive strength using existing and proposed equation.

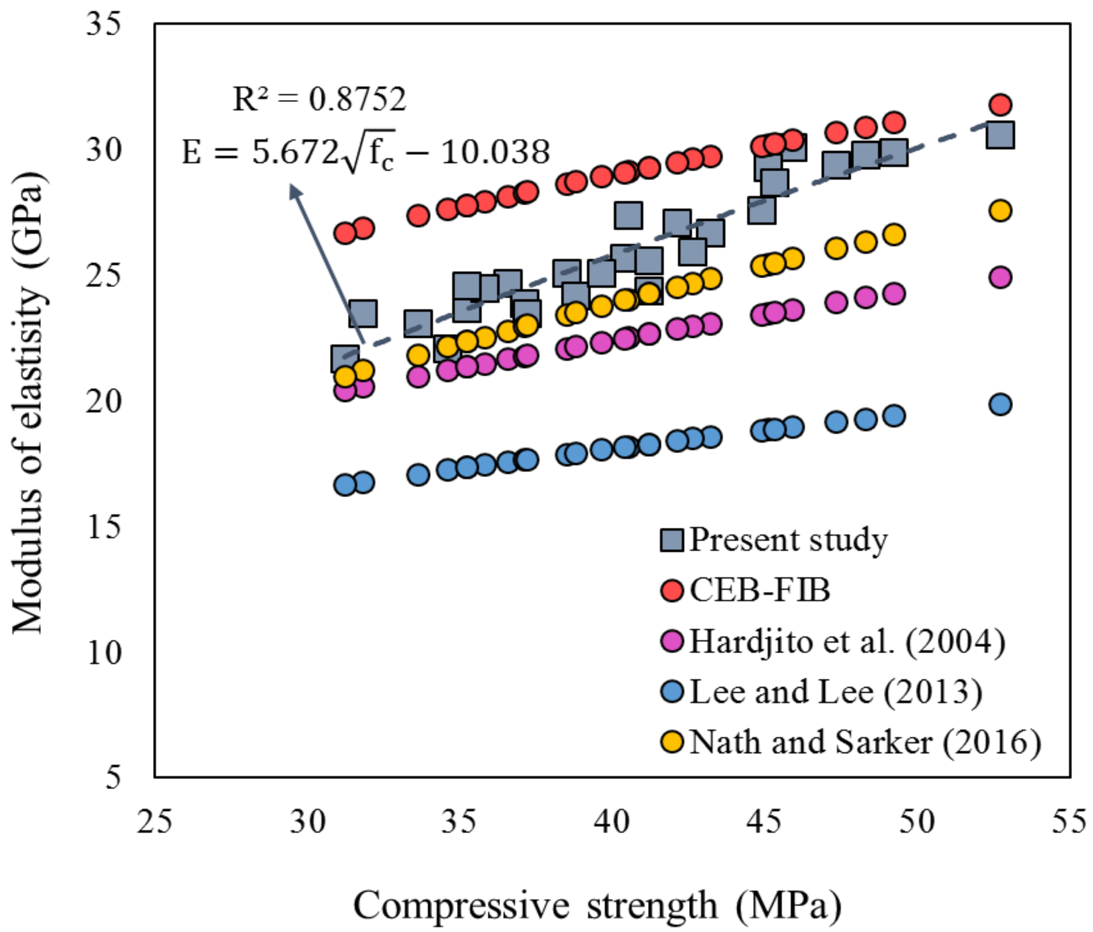

Figure 9. Splitting tensile strength results of HFRGPC versus polypropylene fiber contents.

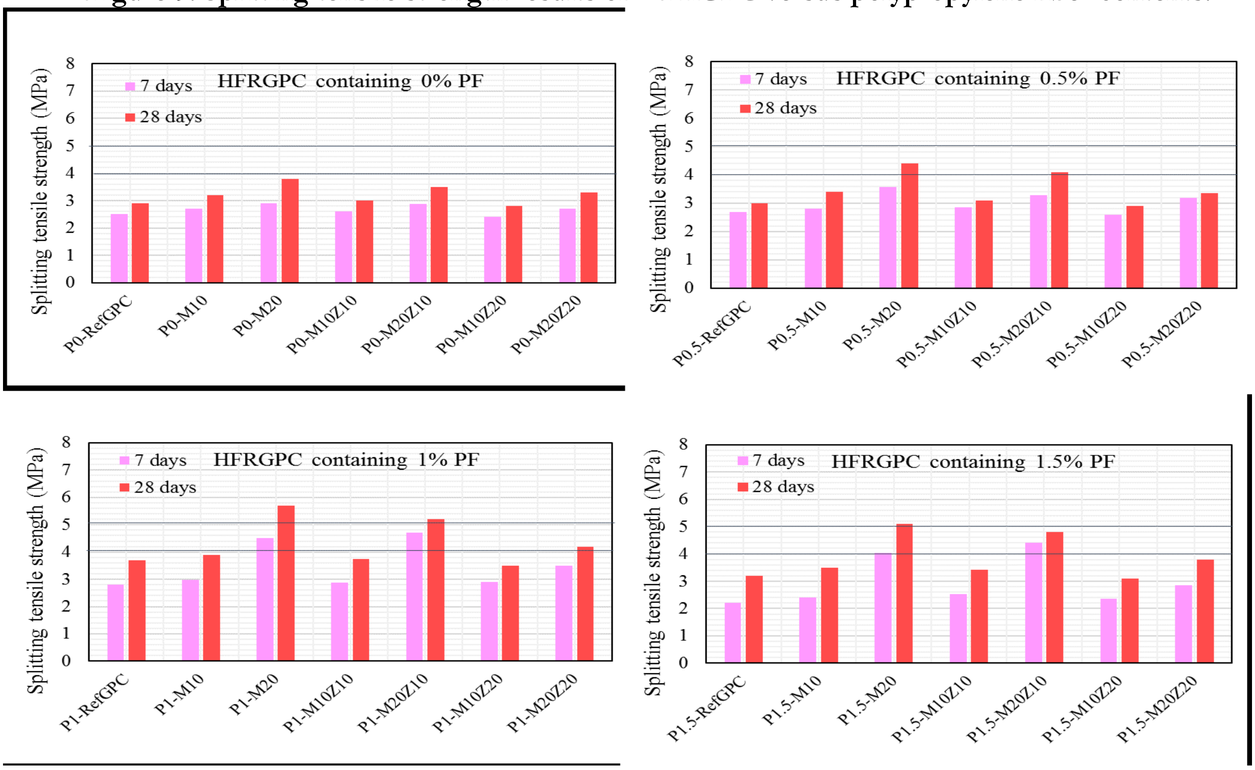

Figure 10. Comparison of experimental and predicted splitting tensile strengths of HFRGPC with different percentages of PF.

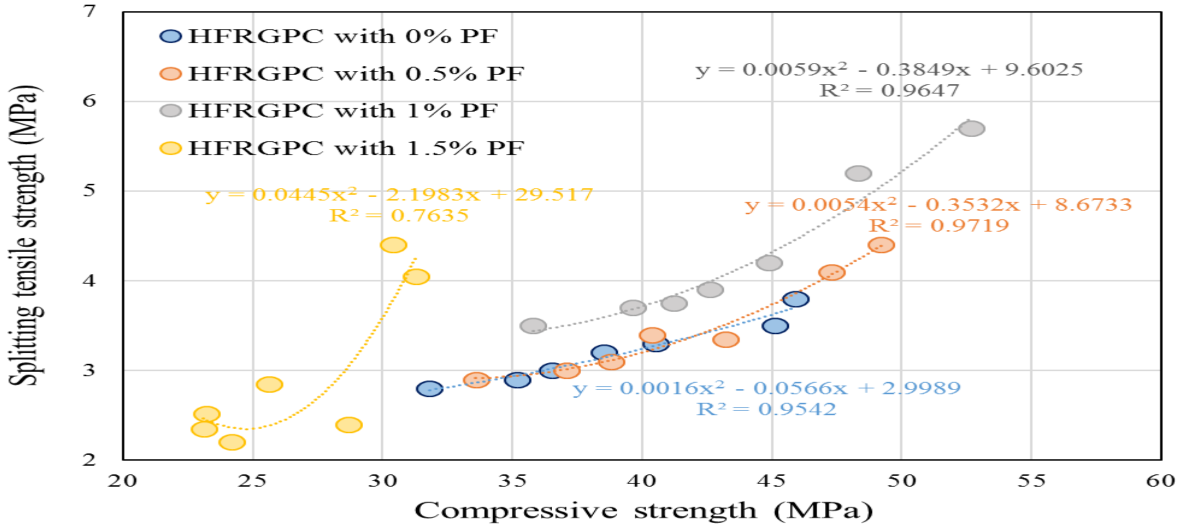

Figure 11. Compressive strength of the HFRGPC specimens exposed to elevated temperatures at 28 days.

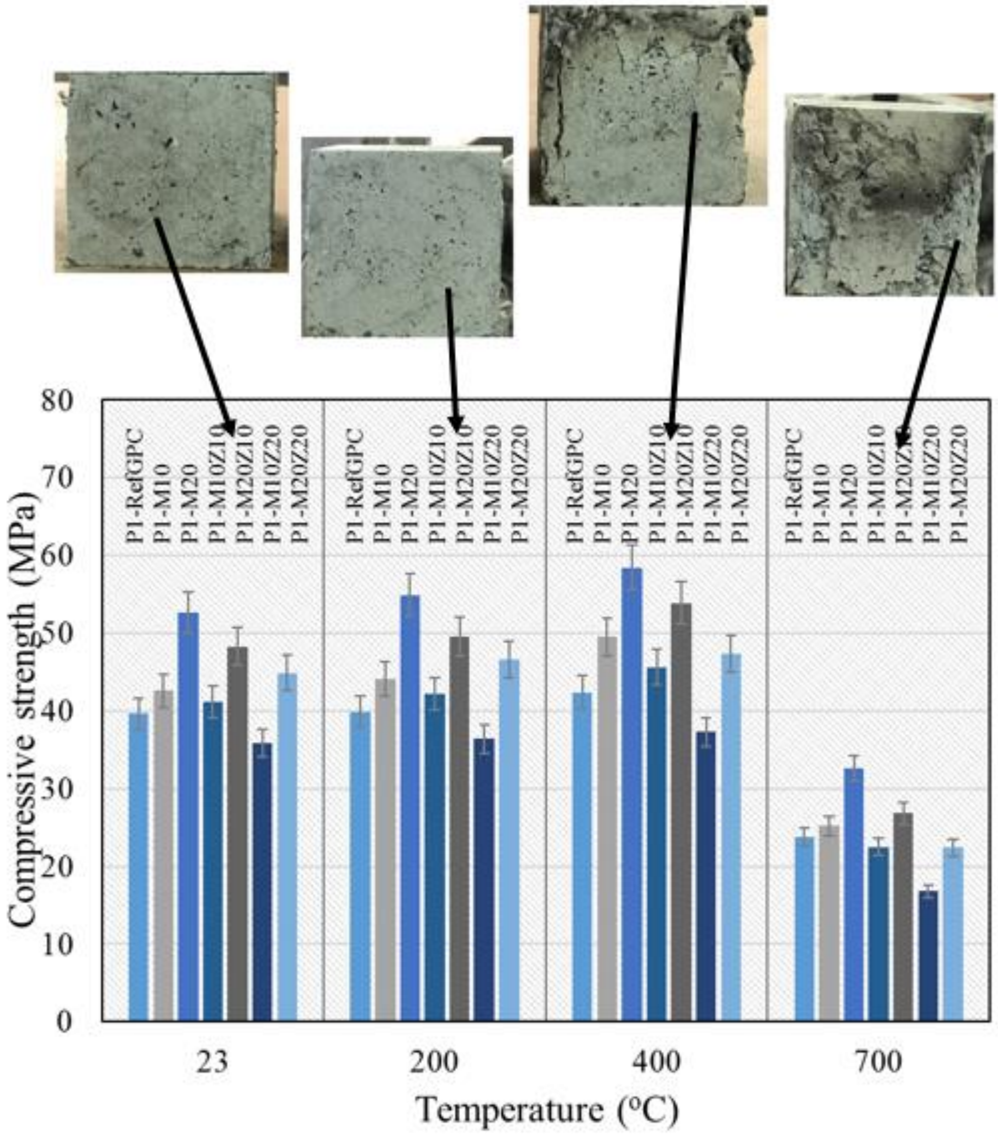

Figure 12. SEM images of HFRGPC specimens before and after exposure to elevated temperatures.

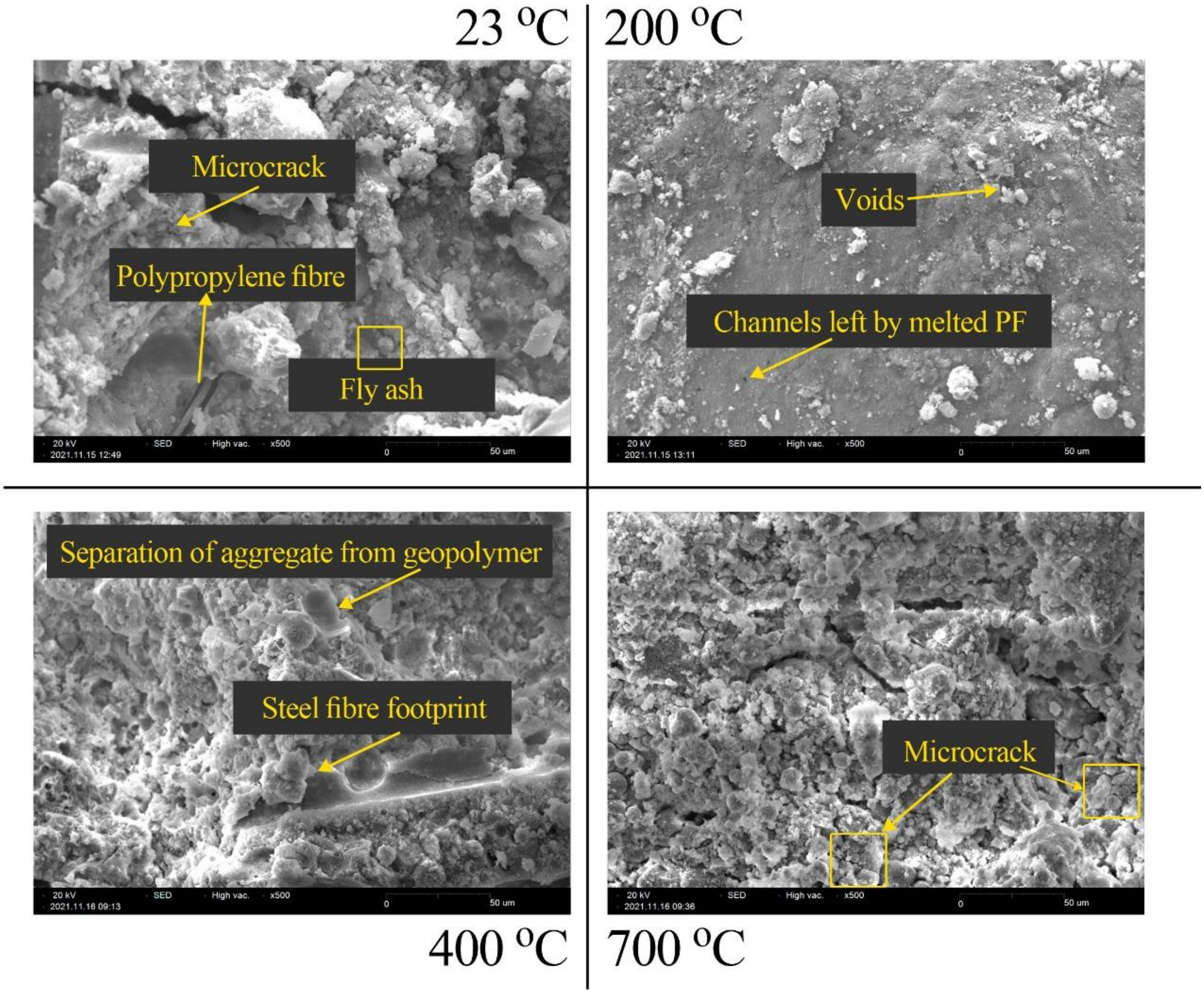

Figure 13. Comparison of observed vs. predicted compressive strength of ML models a) scatter plots b) line graph with relative error.

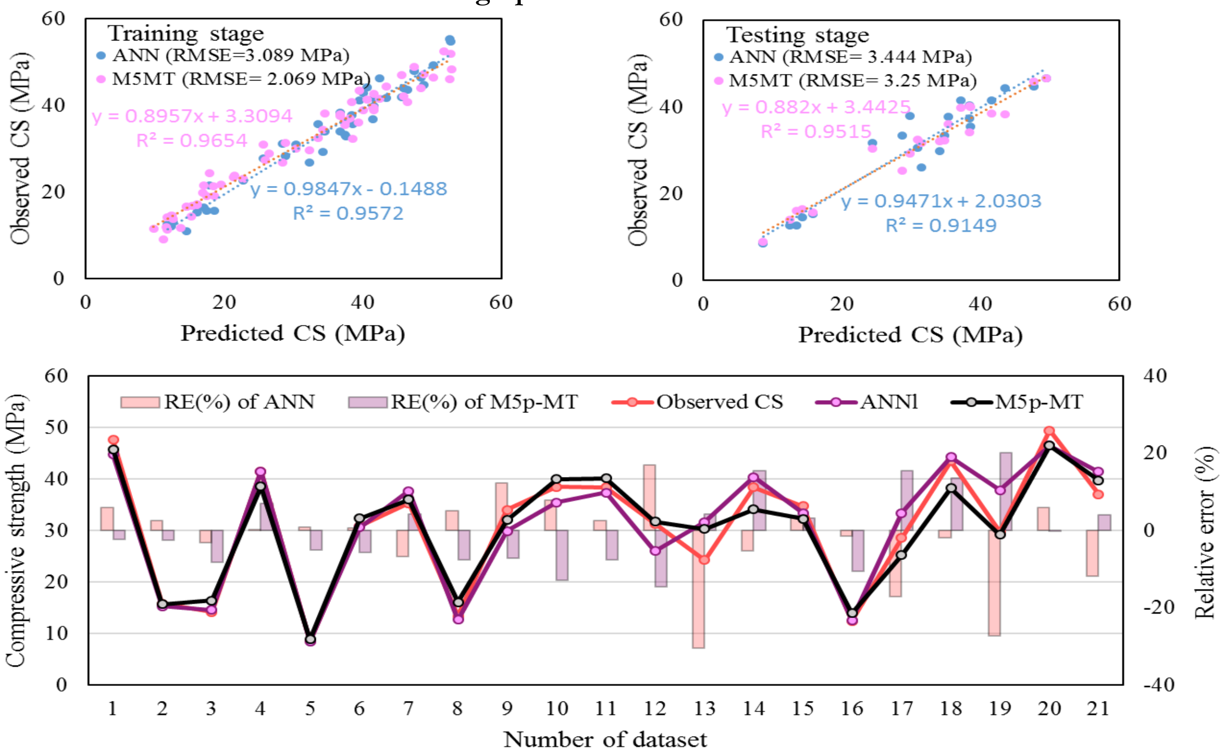

Tables

Table 1. Chemical composition of utilized pozzolanic materials in percentage.

Component (%)	Z	FA	MK
SiO_2	67.79	61.3	52.1
Al_2O_3	13.66	28.8	44.7
Fe_2O_3	1.44	4.98	0.8
CaO	1.68	1.05	0.09
MgO	1.2	0.63	0.03
SO_3	0.5	0.13	-
Na_2O	2.04	0.24	9.1
K_2O	1.42	1.4	0.03
Loss of ignition	10.23	0.7	0.7
Specific gravity	2.3	2.6	2.6
Fineness (m^2/kg)	320	310[a]	12000

Table 2. Characteristics of polypropylene and steel fibers used.

Fiber type	Length (mm)	Density (gr/cm^3)	Tensile strength (MPa)	Water absorbency	Alkaline and acid resistant	Diameter (mm)
PF	6	0.93	400	No	Excellent	-
SF	5	7.8	2500	No	Excellent	0.12

Table 3. Mix proportions of geopolymer concretes.

Mix ID	FAsh (kg/m^3)	MK (kg/m^3)	NZ (kg/m^3)	PF (%)	FA (kg/m^3)	Recycled (kg/m^3)	CA	Na_2SiO_3 (kg/m^3)	NaOH (kg/m^3)
P0-RefGPC	600	0	0	0	525	980		190	95
P0-M10	540	60	0	0	525	980		190	95
P0-M20	480	120	0	0	525	980		190	95
P0-M10Z10	480	60	60	0	525	980		190	95
P0-M20Z10	420	120	60	0	525	980		190	95
P0-M10Z20	420	60	120	0	525	980		190	95
P0-M20Z20	360	120	120	0	525	980		190	95
P0.5-RefGPC	600	0	0	0.5	525	980		190	95
P0.5-M10	540	60	0	0.5	525	980		190	95
P0.5-M20	480	120	0	0.5	525	980		190	95
P0.5-M10Z10	480	60	60	0.5	525	980		190	95
P0.5-M20Z10	420	120	60	0.5	525	980		190	95
P0.5-M10Z20	420	60	120	0.5	525	980		190	95
P0.5-M20Z20	360	120	120	0.5	525	980		190	95
P1-RefGPC	600	0	0	1	525	980		190	95
P1-M10	540	60	0	1	525	980		190	95
P1-M20	480	120	0	1	525	980		190	95
P1-M10Z10	480	60	60	1	525	980		190	95
P1-M20Z10	420	120	60	1	525	980		190	95
P1-M10Z20	420	60	120	1	525	980		190	95
P1-M20Z20	360	120	120	1	525	980		190	95
P1.5-RefGPC	600	0	0	1.5	525	980		190	95
P1.5-M10	540	60	0	1.5	525	980		190	95
P1.5-M20	480	120	0	1.5	525	980		190	95
P1.5-M10Z10	480	60	60	1.5	525	980		190	95
P1.5-M20Z10	420	120	60	1.5	525	980		190	95
P1.5-M10Z20	420	60	120	1.5	525	980		190	95
P1.5-M20Z20	360	120	120	1.5	525	980		190	95

P-MaZa: P refers to the volume fraction of fiber, a represents the percentage of M and Z which are metakaolin and zeolite, respectively. RefGPC containing 100% of flay ash as the referenced specimen.

Table 4. Percentage of residual compressive strength of HFRGPC exposed to different temperatures.

Mix ID	Residual compressive strength (%)		
	200	400	700
P1-RefGPC	100.71	107.02	58.82
P1-M10	103.52	116.20	59.15
P1-M20	104.17	110.91	61.94
P1-M10Z10	102.43	110.68	54.61
P1-M20Z10	102.69	111.59	55.49
P1-M10-Z20	101.68	104.19	46.93
P1-M20-Z20	103.74	105.30	49.89

Table 5. Extracted rules and corresponding equations in M5p-MT model for the prediction of compressive strength of HFRGPC.

Rules	Equations
T <= 650 :	CS1 = 0.0461FAsh + 0.1049MK - 7.2816PF - 0.007T + 13.4021
| MK <= 90 :	CS2 = 0.0436FAsh + 0.1049MK - 7.3883PF - 0.0063T + 14.858
| | PF <= 1.25 :	CS3 = 0.0475FAsh + 0.1049MK - 7.4514PF- 0.007T + 11.3952
| | | FAsh <= 465 : LM1	CS4 = 0.0469FAsh + 0.1049MK - 7.4514PF - 0.007T + 11.8042
| | | FAsh > 465 : LM2	CS5 = 0.0373FAsh + 0.1049 MK- 8.8136PF - 0.0017T + 22.3586
| | PF > 1.25 :	CS6 = 0.0166FAsh - 0.0271NZ + 0.0927MK - 5.2249PF - 0.0148T + 18.7804
| | | FAsh <= 475 : LM3	
| | | FAsh > 475 : LM4	
| MK > 90 : LM5	
T > 650 : LM6	

Table 6. Comparison of the ML model for the prediction of compressive strength of HFRGPC.

ML model	R	RMSE	MAE	U95
ANN-Train	0.98	3.089	2.595	26.91
M5p-MT-Train	0.99	2.069	1.567	25.29
ANN-Test	0.96	3.444	2.514	23.74
M5p-MT-Test	0.97	3.250	2.348	21.17

Table 7. Results of ANOVA for the compressive strength of HFRGPC mixes under high temperature.

Experimental factors	DF	SS	Var	P-value	Contribution (%)
MK (%)	7	1685.5	29.61	0.014	11.65
NZ (%)	2	1722	12.75	0.152	5.52
PF (%)	3	948.9	18.38	0.035	7.73
T (^{o}c)	2	10267	182.97	0.003	71.98
Error	69	701.5	10.09	0.00	2.97
Total	83	14278.1	254.22	-	100